LANGMUIR

Article

pubs.acs.org/Langmuir

Enhanced Dissolution of Liquid Microdroplets in the Extensional Creeping Flow of a Hydrodynamic Trap

Adil Mustafa,[†] Ahmet Erten,[*,†] Rana M. Armaghan Ayaz,[†] Oğuz Kayıllıoğlu,[†] Aysenur Eser,[†] Mustafa Eryürek,[†] Muhammad Irfan,[‡] Metin Muradoglu,[*,‡] Melikhan Tanyeri,[*,¶] and Alper Kiraz[*,†,§]

[†]Department of Physics, [‡]Department of Mechanical Engineering, and [§]Department of Electrical and Electronics Engineering, Koç University, 34450 Sariyer, Istanbul Turkey

[¶]Department of Electrical and Electronics Engineering, Istanbul Sehir University, 34662 Uskudar, Istanbul Turkey

Supporting Information

ABSTRACT: A novel noncontact technique based on hydrodynamic trapping is presented to study the dissolution of freely suspended liquid microdroplets into a second immiscible phase in a simple extensional creeping flow. Benzyl benzoate (BB) and *n*-decanol microdroplets are individually trapped at the stagnation point of a planar extensional flow, and dissolution of single microdroplets into an aqueous solution containing surfactant is characterized at different flow rates. The experimental dissolution curves are compared to two models: (i) the Epstein–Plesset (EP) model which considers only diffusive mass transfer, and (ii) the Zhang–Yang–Mao (ZYM) model which considers both diffusive and convective mass transfer in the presence of extensional creeping flow. The EP model significantly underpredicts the experimentally determined dissolution rates for all experiments. In contrast, very good agreement is observed between the experimental dissolution curves and the ZYM model when the saturation concentration of the microdroplet liquid (c_s) is used as the only fitting parameter. Experiments with BB microdroplets at low surfactant concentration (10 μM) reveal c_s values very similar to that reported in the literature. In contrast, experiments with BB and *n*-decanol microdroplets at 10 mM surfactant concentration, higher than the critical micelle concentration (CMC) of 5 mM, show further enhancements in microdroplet dissolution rates due to micellar solubilization. The presented method accurately tests the dissolution of single microdroplets into a second immiscible phase in extensional creeping flow and has potential for applications such as separation processes, food dispersion, and drug development/design.

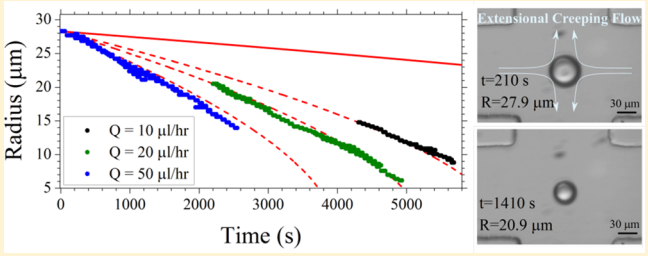

INTRODUCTION

The dissolution of liquid microdroplets is of great importance in many industrial processes with applications ranging from food industry (separation and dispersion) to pharmaceutical industry (drug delivery/design).[1−3] In particular, dissolution is one of the key quality control tests widely used in the pharmaceutical industry. Early work by Epstein and Plesset modeled the diffusion-based dissolution of gas microbubbles in a host liquid.[4] Using a micropipette manipulation technique, Duncan and Needham experimentally verified the Epstein–Plesset (EP) model with single component gas bubbles.[5] Micropipet manipulation was also used to verify the validity of the EP model for single component aniline oil droplets in water[1] and to study the dissolution of multicomponent protein–water microdroplets in water.[6] Recently, the same technique, through a modified form of the EP equation, was used to model the dissolution of microdroplets obtained by a two-component mixture of mutually miscible oils (ethyl acetate, butyl acetate, and amyl acetate) into a second immiscible phase (water).[7]

For liquid microdroplets with extremely low solubilities in the host liquid, experiments that rely on the diffusion-based EP equation can prove to be impractical because of the extended experimental times. For such cases, it is preferable to speed up microdroplet dissolution by incorporating flow into the experiment. In this article, we exploit a novel experimental method, where microdroplets experience extensional creeping flow as they are hydrodynamically trapped. Hydrodynamic trapping is a microfluidic trapping technique where particles are trapped at a stagnation point generated at the junction of two perpendicular microchannels. Recently, hydrodynamic trapping has been introduced as a powerful tool for trapping and manipulation of microbeads, DNA molecules, and cells in microfluidic chips.[8−10] Extensional creeping flow experienced by the hydrodynamically trapped particles is also suitable for performing extensional rheology experiments which allow for high-throughput analysis as compared to other alternatives such as those based on shear flow.[11]

To incorporate the effects of convection due to motion of the host liquid in which the droplet is dissolving, the

Received: June 30, 2016
Revised: August 25, 2016
Published: August 29, 2016

DOI: 10.1021/acs.langmuir.6b02411
Langmuir 2016, 32, 9460−9467

convection−diffusion equation needs to be solved. Kurdyumov and Polyanin studied the effects of convection on droplet dissolution in a shear flow.[12] They used the known analytical solution for the velocity field at small Reynolds number and numerically solved the advection−diffusion equation for the mass transfer for a wide range of Péclet numbers. Péclet number signifies the relative importance of convection compared to diffusion, and is defined as $Pe = UR/D$ where U, R, and D are the free stream velocity, droplet radius, and diffusion coefficient for the droplet liquid in the host fluid. On the basis of their numerical results and the analytical solutions in the limiting cases of very low and very high Pe, they derived a correction relating the Sherwood number to Pe. Sherwood number represents the ratio of the total rate of mass transfer to the rate of purely diffusive mass transport in the absence of convection, and is defined as $Sh = KR/D$, where K is the mass transfer coefficient. This work has been recently extended to the case of extensional creeping flow through extensive numerical simulations by Zhang−Yang−Mao (ZYM).[13]

In this paper, for the first time a novel, noncontact technique based on hydrodynamic trapping is used to study the dissolution of freely suspended benzyl benzoate (BB) and *n*-decanol microdroplets in water. Unlike the micropipette manipulation technique, no mechanical contact is required for trapping of the microdroplets. The studied microdroplets are prepared by vigorous agitation of a solution containing AOT (docusate sodium salt) surfactant at concentrations of 10 μM or 10 mM. Experimental results are compared with the numerical study by ZYM, and good agreements are obtained. Experiments also reveal an enhancement in the dissolution rate of microdroplets due to micellar solubilization when surfactant concentration is increased beyond the critical micelle concentration (CMC).[14,15]

MODELING

The experimental results are compared to the models developed by EP[4] and by ZYM.[13] In both models, the droplet is assumed to remain spherical and dissolution does not alter the material properties of the droplet and host fluids. The EP model only considers diffusive fluxes so it is valid only for small Péclet numbers, i.e., $Pe \ll 1$. The ZYM model takes both the convection and diffusion into account. These two models are briefly explained below and then used to interpret the experimental results in the following section.

Epstein−Plesset (EP) Model. EP model[4] was originally derived for dissolution of single gas bubbles in an infinite domain. Recently, Duncan and Needham[1] have shown that the EP model also applies to dissolution of single liquid droplets in the absence of convection in an infinite domain. According to this model, the dissolution rate of the droplet that can be described as the rate of change in droplet radius (R) with respect to time (t), and is given as

$$\frac{dR}{dt} = -\frac{D(c_s - c_\infty)}{\rho}\left(\frac{1}{R} + \frac{1}{(\pi Dt)^{1/2}}\right) \quad (1)$$

where ρ is the density of the droplet, c_s is the saturation concentration of the droplet liquid in the host fluid, and c_∞ is the concentration of the droplet liquid in the host fluid far away from the droplet (at infinity). Host fluid used in all the experiments reported in this paper did not contain any droplet liquid. Hence c_∞ is assumed to be 0 for all the reported calculations. This model is only valid for diffusion dominated flows, that is, $Pe \ll 1$. Equation 1 is integrated numerically using a 4th order Runge−Kutta method in the present study although EP[4] provided an analytical solution.

Zhang−Yang−Mao (ZYM) Model. Gupalo and Riazantsev[16] were the first to study the convective mass transfer from the surface of a solid sphere and a spherical droplet in a uniform shear flow at high Péclet numbers. They came up with analytical expressions for the mass flux in the approximation of the diffusion boundary layer and showed that Sh is proportional to $Pe^{1/3}$ for a solid sphere and to $Pe^{1/2}$ for a liquid drop. Later, Batchelor[17] derived analytical expressions for the mass transfer rate from a solid sphere suspended in a linear ambient flow field for both low and high Pe. To bridge the gap between low and high Pe analytical solutions, Kurdyumov and Polyanin[12] presented numerical solutions for the mass transfer from spherical particles, drops, and bubbles in a linear creeping shear flow. They also proposed empirical correlations for Sh that fits their numerical calculations very well for $Pe \leq 1000$. ZYM[13] extended this study to a simple extensional creeping flow for a wide range of Péclet numbers (Pe = 1 to 100 000). A numerical study performed by ZYM[13] reveals the following approximate relations for Sh:

$$Sh = \frac{1}{\beta + 1}(0.207Pe^{1/2} - 0.201) + 0.467Pe^{1/2} + 1.053 \quad (2)$$

$$Sh = \frac{1}{\beta + 1}[0.6 + (0.16 + 0.48Pe)^{1/2}] + \frac{\beta}{\beta + 1}[0.5 + (0.125 + 0.745Pe)^{1/3}] \quad (3)$$

eq 2 and eq 3 are valid for $1 \leq Pe \leq 10$ and $10 < Pe \leq 1000$, respectively. β is the ratio of the dynamic viscosity of the droplet to that of the surrounding fluid ($\beta = \mu_d/\mu_s$). The mass transfer rate from the droplet into the ambient fluid is given by,

$$\frac{dm}{dt} = -K(c_s - c_\infty)A_{drop} \quad (4)$$

where A_{drop} is the surface area of the droplet. Substituting $m = (4/3)\ \pi R^3\ \rho$, $A_{drop} = 4\pi R^2$, and $Sh = KR/D$ into eq 4 one obtains

$$\frac{dR}{dt} = -\frac{D(c_s - c_\infty)}{R\rho}Sh \quad (5)$$

Equation 5 together with eq 2 and eq 3 model the dissolution of a microdroplet in simple extensional creeping flow for $1 \leq Pe \leq 1000$. This range of Péclet numbers covers all the experiments presented here. Hence, we will use eqs 2, 3, and 5 to fit to all the data presented in this article. We will use c_s as the fitting parameter since it is not a well-documented parameter of the liquids especially those with very low solubilities.

MATERIALS AND METHODS

Materials and Microdroplet Generation. Two different droplet materials, *n*-decanol ($C_{10}H_{22}O$ and CAS no.112-30-1, 99.0% pure) and benzyl benzoate (BB; $C_{14}H_{12}O_2$ and CAS no.120-51-4, ≥ 99.0% pure), with very small solubilities in water were chosen. Table 1 summarizes relevant material constants of the droplet liquids used in the experiments. All constants are valid at room temperature, at which experiments were performed.

To improve microdroplet stability and prevent microdroplets from sticking on microchannel surfaces, AOT surfactant (Docusate Sodium

DOI: 10.1021/acs.langmuir.6b02411
Langmuir 2016, 32, 9460−9467

Table 1. Droplet Liquid Material Constants

droplet liquid	D (m^2/s)	c_s (kg/m^3)	ρ (kg/m^3)	μ_d (cP)
n-decanol	0.568×10^{-9}[18]	37×10^{-3}[19,20]	0.829[21]	10.9[21]
benzyl benzoate	0.539×10^{-9}[18]	15×10^{-3}[22]	1.112[21]	8.292[23]

Salt, $C_{20}H_{37}NaO_7S$ and CAS No: 577-11-7, ≥ 99.0% pure) was used. In our experiments we used deionized (DI) water with 10 μM or 10 mM AOT surfactant concentrations as the host fluid. Dynamic viscosity of the host fluid was assumed to be that of water, μ_s = 0.89 cP[21] at ∼25 °C. Both of the host fluids were used in the experiments with BB microdroplets while experiments with *n*-decanol microdroplets only employed DI water with 10 mM AOT surfactant as the host fluid. To generate microdroplets, a small amount of microdroplet liquid was added into a glass vial filled with the host liquid. Microdroplets were obtained by subsequent vigorous shaking. After waiting for a short while for the big microdroplets to settle at the bottom of the vial, the solution was loaded into a syringe from the middle of the vial. This sample fluid was subsequently injected into the microfluidic chip using a syringe pump.

Experimental Methods. Hydrodynamic trapping is based on generating a stagnation point at the intersection of two opposing laminar streams. Experimental details on hydrodynamic trapping and manipulation can be found elsewhere.[8−10] An automated feedback control system enables trapping of single particles at the semistable stagnation point. A feedback control loop uses the relative flow rates through the outlet channels as the feedback parameter for stabilizing the position of a target particle at the microchannel junction. Image analysis is used for determining the position of a target particle. The automated feedback control mechanism also enables particle manipulation along the direction of the outlet channels. Hydrodynamic trapping is performed in conventional polydimethylsiloxane (PDMS) microfluidic chips fabricated by multilayer soft lithography. A 35 μm-thick fluidic layer is positioned between a microscope slide and a control layer (see Figure S1 for a height profile measurement performed on the fluidic layer). A thin elastomeric membrane (∼100 μm thickness) separating the control and fluidic layers is deflected down onto the fluidic layer by applying pressure to the control layer, thereby acting as a pneumatic valve, enabling flow rate control through the fluidic layer. Controlling relative flow rates through the outlet channels in the fluidic layer enables us to control the position of the stagnation point and to trap single microdroplets at the junction within the fluidic layer. In Figure 1 we show a layout of the microfluidic chip and the trapping region with an image of a trapped microdroplet.

Experimental Setup. The experimental setup consists of a microfluidic chip, a microscope (Nikon TE-2000 series), a camera (Point Grey Grasshoper3 U3 USB 3.0 CMOS camera), a computer equipped with a data acquisition card (NI USB 6009), a pressure regulator (Proportion-Air DQPV1), a gas tank (Nitrogen), two syringe pumps (Harvard Peristaltic series), and a 4-way valve (Figure 2). Host and sample fluids are injected into the microfluidic chip with syringe pumps. Sample fluid syringe pump contains one syringe whose outlet is connected to the sample fluid inlet of the microfluidic chip. In contrast, host fluid syringe pump contains two syringes whose outlets are connected to two separate host fluid inlets of the microfluidic chip. A custom developed computer program is used to detect microdroplets and find their positions in the trapping region using an image processing algorithm. The program selects and traps the microdroplet that is nearest to the stagnation point. The position of the stagnation point is preset in the program. Once a microdroplet is selected, a feedback loop is activated by controlling the pressure regulator in order to keep the microdroplet trapped at the stagnation point. During the experiments, first, host and sample fluids are injected together into the microfluidic chip in order to make sure that microdroplets are available within the trapping region. Once a microdroplet is trapped, sample fluid flow is turned off using the 4-way valve. This ensures that fluid flow rates coming from left and right inlets are identical during the experiments. A series of snapshots is then recorded with the camera at predetermined time intervals. A microdroplet size at each snapshot is determined by postprocessing the recorded images.

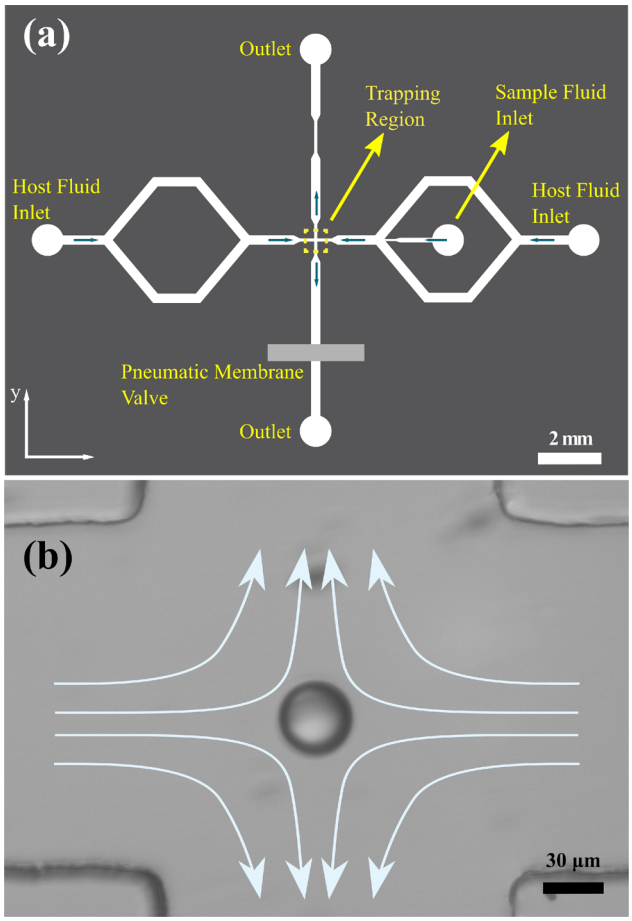

Figure 1. (a) Microfluidic chip layout where inlets, outlets, pneumatic membrane valve and trapping region are indicated. (b) Image of a single microdroplet trapped at the junction of two intersecting microchannels using the hydrodynamic trap. Flow directions in the trapping region are indicated by arrows.

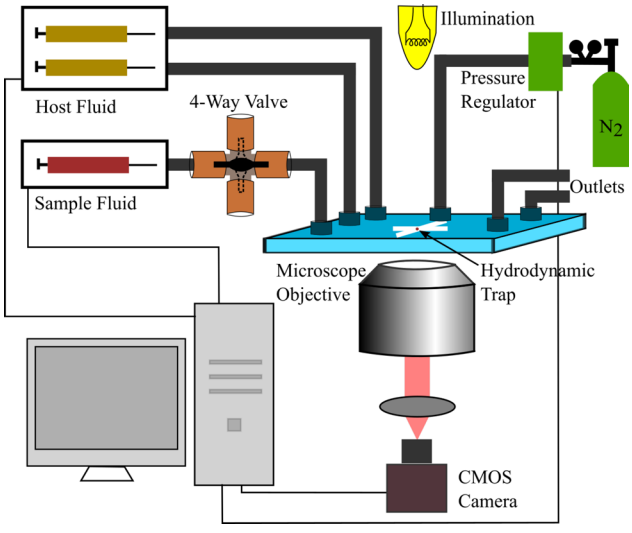

Figure 2. Sketch of the experimental setup used for microdroplet hydrodynamic trapping experiments.

DOI: 10.1021/acs.langmuir.6b02411
Langmuir 2016, 32, 9460−9467

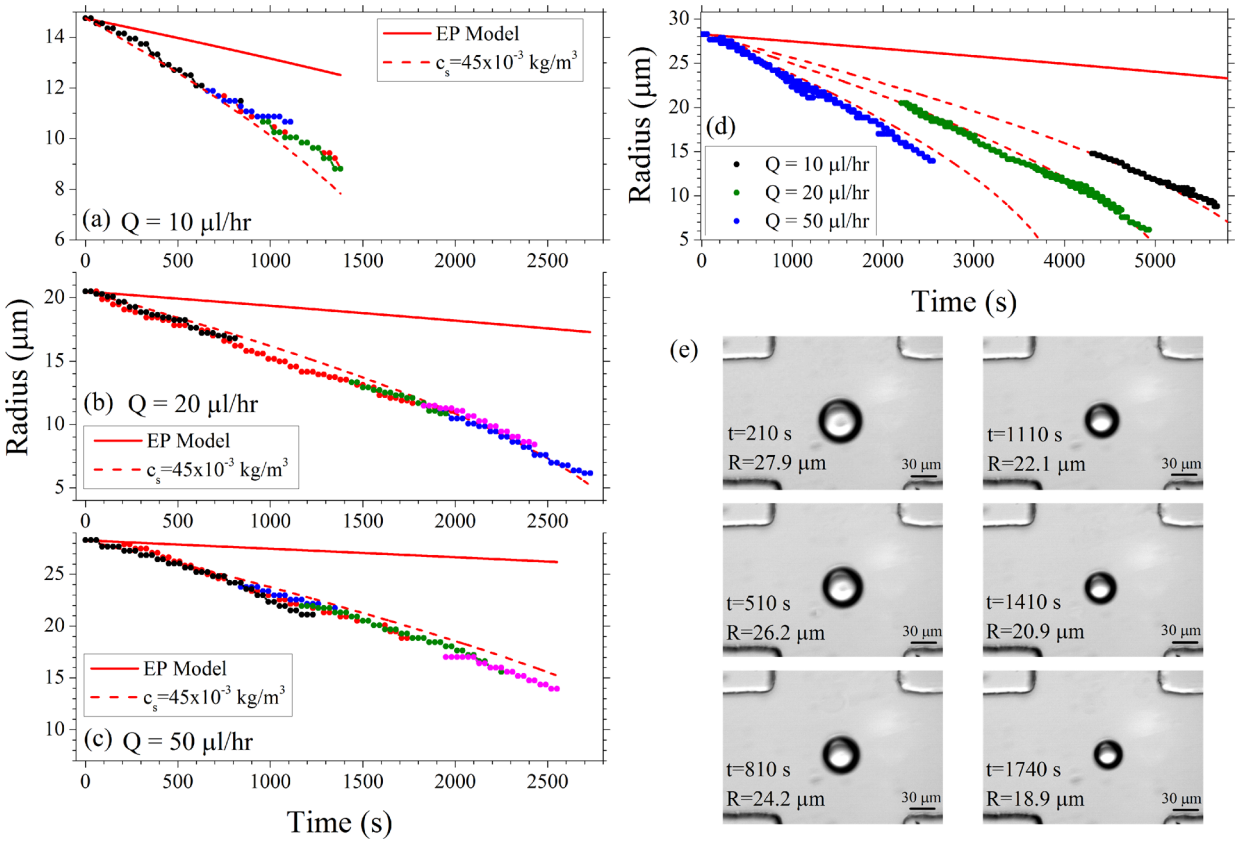

Figure 3. Scatter plots showing dissolution of multiple BB microdroplets in DI water containing 10 mM AOT surfactant at flow rates (a) $Q = 10\ \mu$L/h, (b) $Q = 20\ \mu$L/h, and (c) $Q = 50\ \mu$L/h along with EP and ZYM model predictions. Measurements from 4, 5, and 5 microdroplets are time-shifted to obtain the scatter plots in panels a, b, and c, respectively. (d) Dissolution curves showing the combined scatter plots at three different flow rates along with EP and ZYM model predictions. In panels a–d, solid red lines show the EP model predictions and dashed red lines show the ZYM model predictions assuming $c_s = 45 \times 10^{-3}$ kg/m^3. (e) Snapshot images recorded from an exemplary BB microdroplet while dissolving at a flow rate of $Q = 50\ \mu$L/h (see Movie S1 for a movie of all the recorded images).

Microfluidic Chip Preparation. The microfluidic chips used in our experiments are two layer (PDMS) devices. These two layers, called as fluidic and control layers, are prepared on different silicon molds. PDMS (Sylgard 184, Dow Corning) base to curing agent ratios of 15:1 and 5:1 are used for fluidic and control layers, respectively. After thoroughly mixing the curing agent with base and degassing for 20 min in a desiccator, the fluidic layer mixture is poured over a 3-in. silicon wafer used as the fluidic channel mold. The fluidic channels are designed to have around 35 μm thickness and 150 μm width. A two-step spin coating process (500 rpm for 90 s followed by 750 rpm for 30 s) is applied, and an approximate fluidic layer thickness of 150 μm is achieved. The control layer mixture is first degassed for 20 min in a desiccator and poured over another 3-in. silicon wafer patterned as control layer mold. These two wafers are baked for 40 min at 70 °C, and then the control layer is peeled off from the wafer. After a gas access hole is punched, the PDMS block of the control layer is bonded to the fluidic layer using plasma bonding with a pneumatic pressure membrane carefully placed on the fluidic layer. Thus, the obtained two-layer PDMS block is left at room temperature for 10 min to improve the bonding. Liquid access holes are then punched in the resulting monolithic PDMS structure that is consecutively bonded to a microscope slide using plasma bonding. The final device is left overnight in an oven at 70 °C to improve bonding.

RESULTS AND DISCUSSION

In our experiments, we chose two different droplet materials with very low reported solubilities in water. Specifically, we observed dissolution of BB and *n*-decanol microdroplets into an aqueous solution at various flow rates. BB and *n*-decanol are reported to be insoluble in water in many references in the literature, and there is very limited information about their saturation concentrations in water. Saturation concentrations of BB and *n*-decanol in water are reported to be 15×10^{-3} kg/m^3 and around 37×10^{-3} kg/m^3, respectively.[19,20,22] In our experiments, the aqueous solution was chosen as DI water with AOT surfactant dissolved at 10 μM or 10 mM concentrations.

The results of the microdroplet dissolution experiments together with predictions from EP and ZYM models are shown in Figures 3, 4, and 5 for different volumetric flow rates. These results are described in detail below. Flow rates reported in these experiments correspond to the infusion rates from the host fluid syringe pump. Since two separate syringes are connected to this syringe pump, these infusion rates correspond to flow rates at each inlet channel. They are converted to free stream velocity U using $U = Q/A_{chan}$ where Q is the flow rate and A_{chan} is the cross-sectional area of the fluidic channel that is assumed to be $A_{chan} = 35 \times 150\ \mu$m^2. Table 2 shows the Reynolds numbers calculated for different flow rates used in our experiments. The values shown in this table verify the creeping flow conditions, that is, the Reynolds number being very small ($Re \ll 1$).

Figure 3 shows the results of the microdroplet dissolution experiments performed with BB microdroplets in DI water with 10 mM AOT surfactant concentration at three different flow rates, $Q = 10\ \mu$L/h, $Q = 20\ \mu$L/h, and $Q = 50\ \mu$L/h. Different colors in the scatter plots in Figure 3a–c indicate data recorded

DOI: 10.1021/acs.langmuir.6b02411
Langmuir 2016, 32, 9460–9467

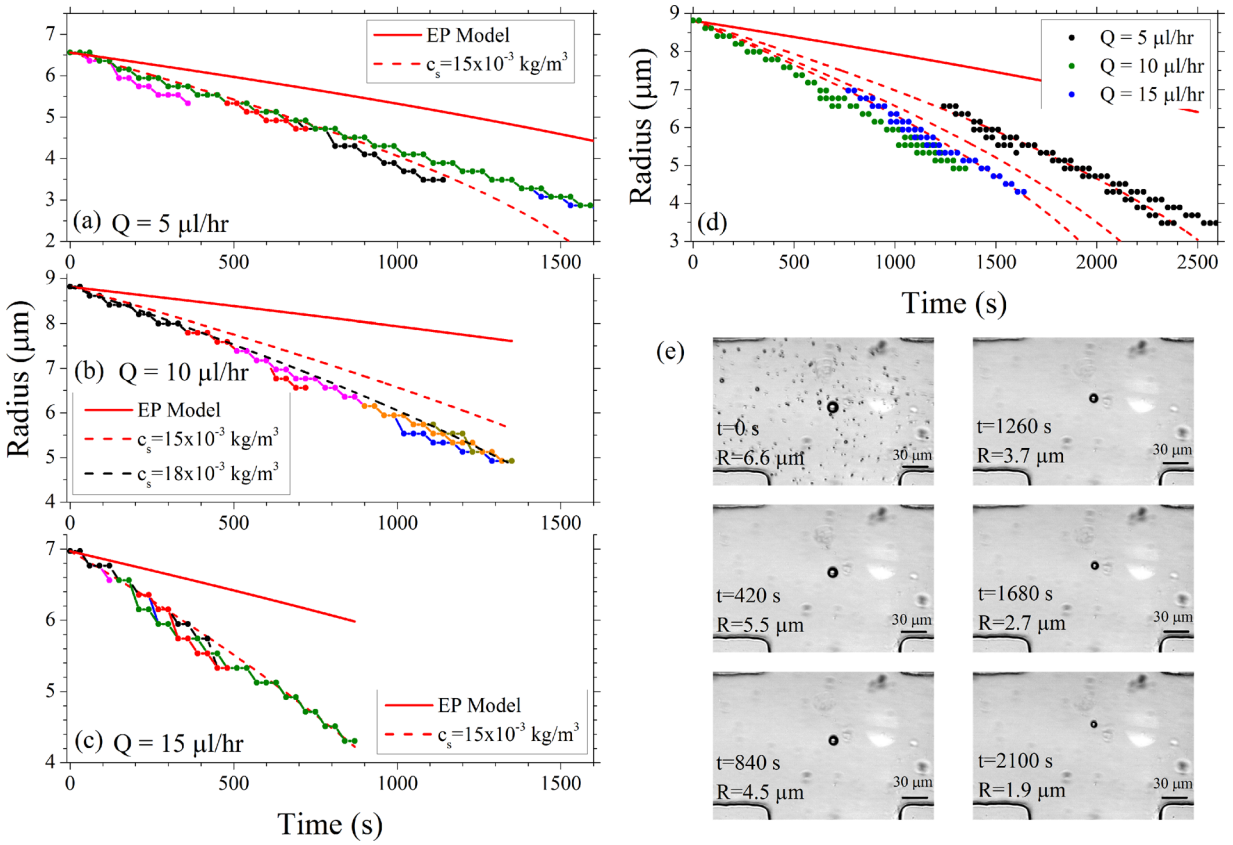

Figure 4. Scatter plots showing dissolution of multiple BB microdroplets in DI water containing 10 μM AOT surfactant at flow rates (a) Q = 5 μL/h, (b) Q = 10 μL/h, and (c) Q = 15 μL/h along with EP and ZYM model predictions. Measurements from 5, 7, and 5 microdroplets are time-shifted to obtain the scatter plots in panels a, b, and c, respectively. (d) Dissolution curves showing the combined scatter plots at three different flow rates along with EP and ZYM model predictions. In panels a–d solid red lines show the EP model predictions and dashed red lines show the ZYM model predictions assuming $c_s = 15 \times 10^{-3}$ kg/m^3. Dashed black line in panel b shows the ZYM model prediciton assuming $c_s = 18 \times 10^{-3}$ kg/m^3. (e) Snapshot images recorded from an exemplary BB microdroplet while at a flow rate of Q = 5 μL/h (see Movie S2 for a movie of all the recorded images).

from different microdroplets. For a certain flow rate, data recorded from each microdroplet is time-shifted such that the initial droplet size has a time stamp that is equal to the time another droplet attains during its dissolution when it has the same size as the initial size of the studied microdroplet. This way continuous-looking scatter plots are obtained. Continuous and smooth nature of the scatter plots in Figure 3a–c suggest that microdroplets examined in this study display consistent dissolution properties. Data recorded from a total number of 4, 5, and 5 microdroplets are shown in Figure 3 panels a, b, and c, respectively. *Pe* and *Sh* values corresponding to these data points as well as other data points presented in Figures 4 and 5 are shown in Figures S2–S4 in the Supporting Information. Solid and dashed lines in Figure 3a–c indicate predictions by the EP and ZYM models. Very good fits are obtained between data and ZYM model predictions if c_s is assumed as $c_s = 45 \times 10^{-3}$ kg/m^3, while keeping all other material constants the same as those provided in Table 1. For each case, the EP model prediction is significantly different than the experimental results, showing the importance of convection-based dissolution in our experiments. The best fit value of c_s with the ZYM model, $c_s = 45 \times 10^{-3}$ kg/m^3, is larger than 15×10^{-3} kg/m^3 reported in the literature.[22] We explain this difference by the enhancement in droplet dissolution rate due to micellar solubilization in the presence of surfactant at a concentration higher than the CMC.[14,15] Micelles are formed when a surfactant is used above its CMC and the process of micelles incorporating solute molecules is called micellar solubilization. For AOT surfactant, CMC value is reported to be 5 mM in water at room temperature.[24] We note that extensional creeping flow is expected to accumulate higher concentration of surfactant molecules at the top and bottom poles of the droplet. Such an inhomogeneous distribution of the surfactant molecules was not considered by the ZYM model, and can cause error in determination of the c_s value. The spherical shape of the droplets will be deformed for droplet sizes larger than the finite thickness (35 μm) of the fluidic channels. This may serve as another source of error in determination of the c_s value using the ZYM model.

In Figure 3d, data collected from different microdroplets are combined and represented by one color for each flow rate. Combined data set for each flow rate is then time-shifted to ensure a good overlap with the ZYM model predictions shown by dashed curves obtained assuming $c_s = 45 \times 10^{-3}$ kg/m^3, while keeping all other material constants the same as those provided in Table 1. This figure shows the enhancement in microdroplet dissolution with the flow rate. For instance at t = 3000 s, droplet radius is observed to decrease by 31%, 39%, and 58%, for Q = 10 μL/h, Q = 20 μL/h, and Q = 50 μL/h, according to the ZYM model. In contrast, the EP model predicts a decrease in droplet radius by only 10% at t = 3000 s.

DOI: 10.1021/acs.langmuir.6b02411
Langmuir 2016, 32, 9460–9467

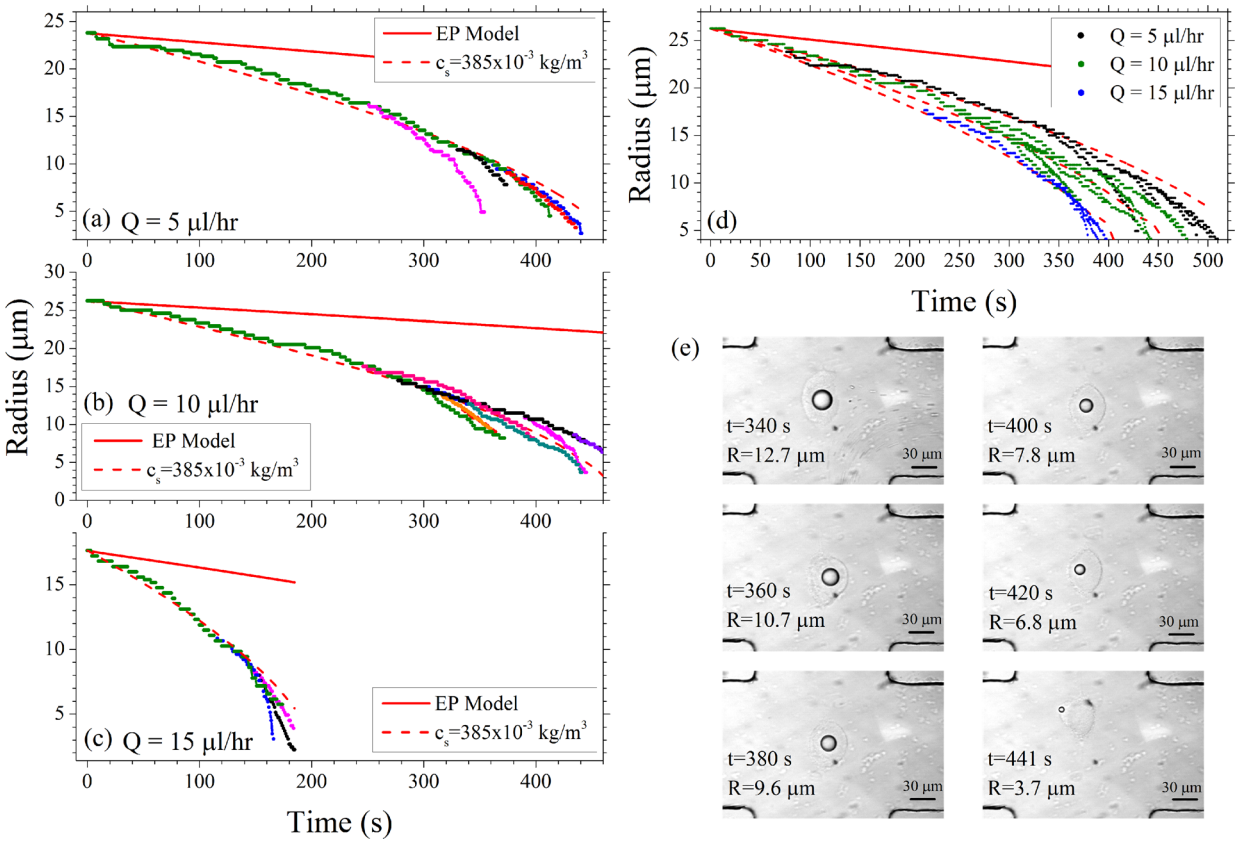

Figure 5. Scatter plots showing dissolution of multiple *n*-decanol microdroplets in DI water containing 10 mM AOT surfactant at flow rates (a) Q = 5 μL/h, (b) Q = 10 μL/h, and (c) Q = 15 μL/h along with EP and ZYM model predictions. Measurements from 5, 9, and 4 microdroplets are time-shifted to obtain the scatter plots in panels a, b, and c, respectively. (d) Dissolution curve showing the combined scatter plots at three different flow rates along with EP and ZYM model predictions. In panels a–d solid red lines show the EP model predictions and dashed red lines show the ZYM model predictions assuming $c_s = 385 \times 10^{-3}$ kg/m^3. (e) Snapshot images recorded from an exemplary *n*-decanol microdroplet while dissolving at a flow rate of Q = 10 μL/h (see Movie S3 for a movie of all the recorded images).

Table 2. *Re* at Corresponding Flow Rate *Q*

Q (μL/h)	*Re*
5	0.016820204
10	0.033640409
15	0.050460613
20	0.067280818
50	0.168202044

Figure 4 shows the results of BB microdroplet dissolution experiments performed in DI water with an AOT surfactant concentration of 10 μM at three different flow rates (Q = 5 μL/h, Q = 10 μL/h, and Q = 15 μL/h). Data collected from 5, 7, and 5 microdroplets are shown in Figure 4 panels a, b, and c, respectively. Red dashed lines in Figure 4a–c indicate the predictions by the ZYM model assuming $c_s = 15 \times 10^{-3}$ kg/m^3, while keeping all other material constants the same as those provided in Table 1. Figure 4d shows the combined scatter plots at different flow rates along with the predictions by EP and ZYM models. Very good fits between the experimental data and the ZYM model predictions are obtained in Figure 4a,c for Q = 5 μL/h and Q = 15 μL/h. For Q = 10 μL/h, a slight deviation is observed between the ZYM model prediction and the measurements if $c_s = 15 \times 10^{-3}$ kg/m^3 is considered. We attribute this deviation mainly to variations in microfluidic chip fabrication that arise during the peeling off process from the molds. For this case, the ZYM model prediction assuming $c_s = 18 \times 10^{-3}$ kg/m^3, shown with the dashed black line curve in Figure 4b, reveals the best fit with the measurements. Hence, our experiments with BB microdroplets in DI water containing 10 μM AOT surfactant reveal $c_s = (15–18) \times 10^{-3}$ kg/m^3. This range of c_s values is in agreement with the previous literature reporting $c_s = 15 \times 10^{-3}$ kg/m^3 in the absence of surfactant.[22] In addition, in this case, the AOT surfactant concentration is less than the CMC of 5 mM;[24] hence, the presence of AOT surfactant at 10 μM concentration is not expected to significantly change the droplet dissolution, and the observed c_s value remains around 15×10^{-3} kg/m^3 which is identical to the case in which the host liquid does not contain any surfactant.

We observed dissolution of *n*-decanol microdroplets in DI water containing 10 mM AOT surfactant at three different flow rates (Q = 5 μL/h, Q = 10 μL/h, and Q = 15 μL/h). Results of these experiments are shown in Figure 5 along with the predictions by EP and ZYM models. Data collected from 5, 9, and 4 microdroplets are shown in different colors in Figure 5 panels a, b, and c, respectively. For all flow rates, good fits are obtained between the experimental data and ZYM model predictions if c_s is assumed as 385×10^{-3} kg/m^3, while keeping all other material constants the same as those provided in Table 1. Combined scatter plots at each flow rate are plotted in Figure 5d along with the predictions by EP and ZYM models. Similar to the case of BB microdroplets in DI water containing 10 mM AOT surfactant (Figure 3), in this case, the best fitting c_s value

DOI: 10.1021/acs.langmuir.6b02411
Langmuir 2016, 32, 9460–9467

is larger than 37×10^{-3} kg/m^3, reported in the literature in the absence of surfactant.[19,20] We explain the observed increase in the c_s value by the presence of the AOT surfactant at a concentration higher than the CMC of 5 mM.[24]

In the experiments shown in Figure 5, "halos" surrounding the microdroplet image were always observed. We attribute this to the accumulation of a gelled phase compound of surfactant molecules, micelles, and semidilute microdroplets around the trapped microdroplet due to the high surfactant concentration. These halos morph over time as the microdroplets dissolve. The sequence of images in the inset of Figure 5 shows the deformation of the halo structure as a microdroplet dissolves. The ZYM model does not take into account the presence of such an additional layer on the microdroplet surface. Hence, the presence of the halo structure could explain the deviation of the dissolution curves from the ZYM model predictions for some microdroplets.

From an experimental perspective, working at lower surfactant concentration proved to be difficult. In particular, working at lower surfactant concentrations limited the stability of microdroplet solution to tens of minutes compared to days at higher surfactant concentrations. Moreover, since droplets have a relatively long distance to travel before reaching the stagnation point, reduced surfactant concentrations increased the adhesion of droplets on channel surfaces. As a result, the dissolution of *n*-decanol microdroplets in host liquid containing 10 μM AOT surfactant could not be studied. Similarly, for the case of BB microdroplets, only relatively small microdroplet sizes ($R < 9$ μm) could be studied with 10 μM surfactant concentration in the host fluid (Figure 4).

CONCLUSION

The dissolution of BB and n-decanol microdroplets into an aqueous phase in an extensional creeping flow was studied using a novel noncontact technique based on hydrodynamic trapping under well-defined solution and flow conditions. The experimental dissolution results were compared to EP and ZYM model predictions. In general, the ZYM model was found to be a good approximation for predicting the enhanced dissolution rate of microdroplets due to the convective mass transfer by the extensional creeping flow. The EP model that only considers diffusion mass transfer was found to underpredict the dissolution rate of microdroplets. The use of different surfactant concentrations to control the microdroplet stability was shown to affect the microdroplet dissolution rate. Best fit of the ZYM model to the measurements with BB droplets at 10 mM AOT surfactant concentration revealed a saturation concentration (c_s) of 45×10^{-3} kg/m^3. In contrast, at 10 μM AOT surfactant concentration the best fit revealed $c_s = (15-18) \times 10^{-3}$ kg/m^3, very close to 15×10^{-3} kg/m^3 reported in the literature in the absence of surfactant.[22] Similarly, best fit of the ZYM model to the experiments with *n*-decanol microdroplets at 10 mM AOT surfactant concentration revealed $c_s = 385 \times 10^{-3}$ kg/m^3 while the values reported in literature are around 37×10^{-3} kg/m^3 in the absence of surfactant.[19,20] Hence for both BB and *n*-decanol, micellar solubilization[14,15] was observed to further enhance dissolution rates with surfactant concentrations beyond the critical micelle concentration (CMC) of 5 mM.[24] The method using the ZYM model presented in this work proved to be accurate to test the dissolution of single microdroplets into a second immiscible phase in extensional creeping flow. The demonstrated method has great potential for fundamental studies in modeling droplet dissolution and for industrial applications such as separation processes, food dispersion, and drug development/design. In our experiments, the main limitations on the validity of the ZYM model are posed by the inhomogeneous surfactant distribution on the droplet surface, and droplet deformation perpendicular to the flow direction caused by the finite thickness of the fluidic channels. For the cases studied, no significant droplet deformation was induced along the flow directions by the extensional creeping flow. However, dissolution studies using low surface tension microdroplets with enhanced deformability are currently in progress.

ASSOCIATED CONTENT

Supporting Information

The Supporting Information is available free of charge on the ACS Publications website at DOI: 10.1021/acs.langmuir.6b02411.

Dissolution of a hydrodynamically trapped benzyl benzoate microdroplet in DI water containing 10 mM AOT surfactant at a flow rate of $Q = 50$ μL/h, video consists of 52 images recorded with 30 s interval (AVI)

Dissolution of a hydrodynamically trapped benzyl benzoate microdroplet in DI water containing 10 mM AOT surfactant at a flow rate of $Q = 5$ μL/h, video consists of 102 images recorded with 1 s interval (AVI)

Dissolution of a hydrodynamically trapped *n*-decanol microdroplet in DI water containing 10 mM AOT surfactant at a flow rate of $Q = 10$ μL/h, video consists of 102 images recorded with 1 s interval (AVI)

Profilometer measurement showing the height of the SU-8 mold used for the fluidic layer, *Pe* and *Sh* values calculated for data points presented in Figures 3−5 (PDF)

AUTHOR INFORMATION

Corresponding Authors

*E-mail: ahmeterten@gmail.com.
*E-mail: mmuradoglu@ku.edu.tr.
*E-mail: melikhantanyeri@sehir.edu.tr.
*E-mail: akiraz@ku.edu.tr.

Notes

The authors declare no competing financial interest.

ACKNOWLEDGMENTS

This work was supported by Koç University Seed Funding Program (Grant No. SF.00007) and TÜBİTAK (Grant No. 115S120). The authors thank A. L. Demirel for useful discussions.

REFERENCES

(1) Duncan, P. B.; Needham, D. Microdroplet dissolution into a second-phase solvent using a micropipet technique: test of the Epstein-Plesset model for an aniline-water system. *Langmuir* **2006**, *22*, 4190−4197.

(2) Harland, R. S.; Gazzaniga, A.; Sangalli, M. E.; Colombo, P.; Peppas, N. A. Drug/polymer matrix swelling and dissolution. *Pharm. Res.* **1988**, *5*, 488−494.

(3) O'Donnell, P. B.; McGinity, J. W. Preparation of microspheres by the solvent evaporation technique. *Adv. Drug Delivery Rev.* **1997**, *28*, 25−42.

(4) Epstein, P.; Plesset, M. On the Stability of Gas Bubbles in Liquid-Gas Solutions. *J. Chem. Phys.* **1950**, *18*, 1505−1509.

DOI: 10.1021/acs.langmuir.6b02411
Langmuir 2016, 32, 9460−9467

(5) Duncan, P. B.; Needham, D. Test of the Epstein-Plesset model for gas microparticle dissolution in aqueous media: Effect of surface tension and gas undersaturation in solution. *Langmuir* **2004**, *20*, 2567−2578.
(6) Rickard, D. L.; Duncan, P. B.; Needham, D. Hydration Potential of Lysozyme: Protein Dehydration Using a Single Microparticle Technique. *Biophys. J.* **2010**, *98*, 1075−1084.
(7) Su, J. T.; Needham, D. Mass Transfer in the Dissolution of a Multicomponent Liquid Droplet in an Immiscible Liquid Environment. *Langmuir* **2013**, *29*, 13339−13345.
(8) Tanyeri, M.; Johnson-Chavarria, E. M.; Schroeder, C. M. Hydrodynamic trap for single particles and cells. *Appl. Phys. Lett.* **2010**, *96*, 224101.
(9) Tanyeri, M.; Ranka, M.; Sittipolkul, N.; Schroeder, C. M. A microfluidic-based hydrodynamic trap: design and implementation. *Lab Chip* **2011**, *11*, 1786−1794.
(10) Tanyeri, M.; Schroeder, C. M. Manipulation and Confinement of Single Particles Using Fluid Flow. *Nano Lett.* **2013**, *13*, 2357−2364.
(11) Tse, H. T. K.; Gossett, D. R.; Moon, Y. S.; Masaeli, M.; Sohsman, M.; Ying, Y.; Mislick, K.; Adams, R. P.; Rao, J.; Di Carlo, D. Quantitative Diagnosis of Malignant Pleural Effusions by Single-Cell Mechanophenotyping. *Sci. Transl. Med.* **2013**, *5*, 212ra163−212ra163.
(12) Kurdyumov, V.; Polyanin, A. Mass transfer problem for particles, drops and bubbles in a shear flow. *Fluid Dyn.* **1990**, *25*, 611−615.
(13) Zhang, J.; Yang, C.; Mao, Z.-S. Mass and heat transfer from or to a single sphere in simple extensional creeping flow. *AIChE J.* **2012**, *58*, 3214−3223.
(14) Gentle, I.; Barnes, G. *Interfacial Science: An Introduction*; Oxford University Press, 2005.
(15) Rangel-Yagui, C.; Pessoa, A.; Tavares, L. Micellar solubilization of drugs. *J. Pharm. Pharm. Sci.* **2005**, *8*, 147−163.
(16) Gupalo, P.; Riazantsev, S. Diffusion on a particle in the shear ow of a viscous fluid. Approximation of the diffusion boundary layer. *J. Appl. Math. Mech.* **1972**, *36*, 447−451.
(17) Batchelor, G. Mass transfer from a particle suspended in fluid with a steady linear ambient velocity distribution. *J. Fluid Mech.* **1979**, *95*, 369−400.
(18) Yaws, C. L. *Transport Properties of Chemicals and Hydrocarbons*; William Andrew, 2014.
(19) Yaws, C. L.; Hopper, J. R.; Sheth, S. D.; Han, M.; Pike, R. W. Solubility and Henry's law constant for alcohols in water. *Waste Manage.* **1997**, *17*, 541−547.
(20) Barton, A. F. *Alcohols with Water: Solubility Data Series*; Elsevier, 2013.
(21) Lide, D. *CRC Handbook of Chemistry and Physics 2004−2005: A Ready-Reference Book of Chemical and Physical Data*; CRC, 2004.
(22) Drugbank, Benzyl Benzoate. 1999; http://www.drugbank.ca/drugs/DB00676 (accessed: 2016-05-21).
(23) Riddick, J.; Bunger, W.; Sakano, T. *Organic Solvents*, 4th ed.; Techniques of Chemistry, Volume *II*; Wiley, 1985.
(24) Remington, J. P.; Troy, D. B.; Beringer, P. *Remington: The science and practice of pharmacy*; Lippincott Williams & Wilkins, 2006; Vol. *1*.

DOI: 10.1021/acs.langmuir.6b02411
Langmuir 2016, 32, 9460−9467